Engineering genetic devices for in vivo control of therapeutic T cell activity triggered by the dietary molecule resveratrol

Linfeng Yang[a], Jianli Yin[a], Jiali Wu[a], Longliang Qiao[a], Evan M. Zhao[b], Fengfeng Cai[c], and Haifeng Ye[a,1]

[a]Synthetic Biology and Biomedical Engineering Laboratory, Biomedical Synthetic Biology Research Center, Shanghai Key Laboratory of Regulatory Biology, Institute of Biomedical Sciences and School of Life Sciences, East China Normal University, Shanghai 200241, China; [b]Wyss Institute for Biologically Inspired Engineering, Harvard University, Boston, MA 02215; and [c]Department of Breast Surgery, Yangpu Hospital, School of Medicine, Tongji University, Shanghai 200090, China

Edited by David A. Weitz, Harvard University, Cambridge, MA, and approved July 13, 2021 (received for review April 7, 2021)

Chimeric antigen receptor (CAR)–engineered T cell therapies have been recognized as powerful strategies in cancer immunotherapy; however, the clinical application of CAR-T is currently constrained by severe adverse effects in patients, caused by excessive cytotoxic activity and poor T cell control. Herein, we harnessed a dietary molecule resveratrol (RES)–responsive transactivator and a transrepressor to develop a repressible transgene expression (RES_{rep}) device and an inducible transgene expression (RES_{ind}) device, respectively. After optimization, these tools enabled the control of CAR expression and CAR-mediated antitumor function in engineered human cells. We demonstrated that a resveratrol-repressible CAR expression (RES_{rep}-CAR) device can effectively inhibit T cell activation upon resveratrol administration in primary T cells and a xenograft tumor mouse model. Additionally, we exhibit how a resveratrol-inducible CAR expression (RES_{ind}-CAR) device can achieve fine-tuned and reversible control over T cell activation via a resveratrol-titratable mechanism. Furthermore, our results revealed that the presence of RES can activate RES_{ind}-CAR T cells with strong anticancer cytotoxicity against cells in vitro and in vivo. Our study demonstrates the utility of RES_{rep} and RES_{ind} devices as effective tools for transgene expression and illustrates the potential of RES_{rep}-CAR and RES_{ind}-CAR devices to enhance patient safety in precision cancer immunotherapies.

synthetic biology | genetic switch | CAR-T therapy | resveratrol | cancer immunotherapy

T cell therapy with tumor-targeted chimeric antigen receptor (CAR)–engineered T cells has proven to be a transformative cancer treatment for a range of target indications (1, 2). CARs are constructed via a surface-displayed single-chain antibody variable domain (scFv) coupled to intracellular signaling components, to endow patient-derived T cells with the ability to recognize antigens and subsequently eliminate tumor cells (3). Ever since the approval of CD19-specific CAR T cells for the treatment of B cell leukemias and lymphomas, dramatic clinical successes have been achieved and numerous CAR T cell products are emerging (4–7).

Despite initial encouraging results, several challenges remain for CD19 CAR T cells, one main challenge being a lack of control over these engineered cells (8, 9). Rapid responses after large cell infusion doses can induce several immune-mediated side effects, such as cytokine release syndrome (CRS), tumor lysis syndrome, and neurotoxicity (10, 11). However, achieving potent therapeutic effects requires the robust expansion and sequential activation of a sufficient number of CAR T cells. Accordingly, it is a significant challenge to administrate appropriate doses of this "living drug" in order to balance in vivo efficacy and toxicity, further complicated by the highly divergent responses of patients (12–14).

Synthetic devices have been shown to improve the safety and feasibility of CAR T cell therapy by regulating CAR expression and controlling T cell activation (15, 16). To mitigate immunotherapy toxicity, several safety devices have been developed to control engineered T cells in a "function-off" or "function-on" manner. Previous studies have reported several user-controlled function-off devices to eliminate infused T cells from patients exhibiting severe toxicity, including suicide devices (17, 18), antibody-based elimination devices (9, 19, 20), small molecule-controlled STOP-CAR devices (21), and photoswitchable CAR devices (22). However, function-off devices may be insufficient to ensure safety against toxicities induced immediately upon cell infusion.

Complementary strategies using a function-on approach include several inducible devices with tunable CAR T cell function control: small molecule-inducible CAR devices (23–27), intermediary antibody or protein-based CAR devices (28–30), as well as light/ultrasound-responsive noninvasive devices (31–33). Synthetic Notch (synNotch) receptor-based circuits were also designed to enhance the precision of tumor recognition (34–38). Although these devices theoretically enable safer CAR T cell therapies, synthetic modules controlled by even safer natural molecules capable of diffusing throughout the entire body would offer a more versatile mechanism of control. Further development of orthogonally regulated devices that enable facile control of CAR T cell

Significance

Chimeric antigen receptor (CAR)–engineered T cell therapies have shown tremendous success in the clinic, but excessive cytotoxic activity and poor control over engineered T cells limit the application of CAR-T therapies. Here we have developed resveratrol (RES)–triggered regulation devices (on/off) that could be installed into CAR-T cells, which allow precise control over T cell activity through adjustment of RES dosage. We further demonstrated RES-inducible/repressible CAR expression and reversible control over T cell activation via a RES-titratable mechanism. Our results reveal that RES_{ind}-CAR T cells can be dose-dependently activated by RES with strong anticancer cytotoxicity. Our RES-controlled systems establish proof of concept for strategies to control cancer immunotherapies based on the RES-regulated repression/induction of therapeutic immune cells.

Author contributions: H.Y. conceived the project; L.Y. and H.Y. designed research; L.Y., J.Y., J.W., and L.Q. performed research; L.Y., J.Y., E.M.Z., F.C., and H.Y. analyzed data; and L.Y., J.Y., E.M.Z., F.C., and H.Y. wrote the paper.

Competing interest statement: H.Y., L.Y., and J.Y. are inventors of patent applications (Chinese patent application no. 202110671259.9) submitted by East China Normal University that covers the RES_{rep} and RES_{ind} devices.

This article is a PNAS Direct Submission.

[1]To whom correspondence may be addressed. Email: hfye@bio.ecnu.edu.cn.

This article contains supporting information online at https://www.pnas.org/lookup/suppl/doi:10.1073/pnas.2106612118/-/DCSupplemental.

Published August 17, 2021.

functions to ensure safer device control in immunotherapy is needed.

The stilbenoid natural product resveratrol (RES, 3,4′,5-trihydroxystilbene), notably present in red wine, grapes, peanuts, and berries, has been shown to be a safe inducer compound for genetic devices designed for therapeutic applications (39). Beyond its demonstrated utility in genetic engineering applications, this molecule possesses wide-ranging beneficial effects, including clinical evidence for activities against aging, cancer, cardiovascular diseases, and inflammation (40–43).

To enable safer strategies for cancer immunotherapy with both a function-off and function-on modality, we designed a resveratrol-repressible transgene expression (RES_{rep}) device and a resveratrol-inducible transgene expression (RES_{ind}) device based on resveratrol-responsive regulatory elements. We demonstrate that our RES_{rep} and RES_{ind} devices can reversibly and flexibly control transgene expression in vitro and in vivo in a highly tunable manner. We further apply these devices to control CAR expression and CAR-mediated cell activities by developing a resveratrol-repressible CAR expression (RES_{rep}-CAR) device and a resveratrol-inducible transgene expression (RES_{ind}-CAR) device. We then demonstrate that the RES_{rep}-CAR device can repress CAR expression and CAR-mediated cell activation in primary human T cells and a xenograft mouse model of leukemia, all with triggerable T cell inactivity in case of severe toxicity. We further confirm the titratable and reversible capabilities of the RES_{ind}-CAR device for both CAR expression and T cell activity in vitro and in vivo; this is a feature that could allow physicians to precisely control T cell activity by adjusting the dosage of resveratrol according to the clinical responses of individual patients. These resveratrol-controlled transgene expression devices extend synthetic biology-inspired tools to clinically relevant applications and provide potential strategies for improving the safety of T cell immunotherapies by preventing fatal toxicity in clinical settings.

Results

Design, Construction, and Characterization of an RES_{rep} Device in Mammalian Cells and Mice. Capitalizing on resveratrol-responsive TtgR, a specific transcriptional repressor of efflux pump (TtgABC) in *Pseudomonas putida* (44), we engineered a RES_{rep} device in mammalian cells (Fig. 1*A*). Our designed RES_{rep} device consists of a resveratrol-dependent transactivator $ResA_3$ (TtgR-VPR) that we fused to a synthetic activator VPR (comprising three transcriptional activators: VP64, p65, and Rta) (45) via the C terminus of TtgR. The chimeric transactivator can bind to the resveratrol-dependent promotor P_{ResA1}, which contains a $ResA_3$ binding site (O_{TRC1}, reverse complement and site-directional mutation of O_{TtgR}) positioned in front of a minimal human cytomegalovirus immediate-early promoter ($P_{hCMVmin}$). Transactivator binding results in recruitment of the transcription initiation complex to trigger transgene expression; subsequently, resveratrol releases $ResA_3$ from P_{ResA1}, thereby silencing transgene expression (Fig. 1*A*).

We initially optimized the synthetic transactivator ResA by fusing TtgR to different transactivation domains (VP16, VP64, and VPR) driven by P_{SV40} (simian virus 40 promoter) or P_{hCMV} (human cytomegalovirus promoter; *SI Appendix*, Fig. S1 *A–H*) as well as optimizing the promoter P_{ResA} with various iterations of O_{TRC1} tandem repeats (*SI Appendix*, Fig. S1 *I–N*). Ultimately, we found that a combination of P_{hCMV}-driven $ResA_3$ and P_{ResA1}-driven secreted human placental alkaline phosphatase (SEAP) demonstrated the best induction performance; this version of the RES_{rep} device also achieved significant induction performance in five human cell lines (Fig. 1*B*). Importantly, assessment of resveratrol-mediated toxicity in mammalian cells showed that resveratrol had no negative effect on cell viability (*SI Appendix*, Fig. S2), using resveratrol concentrations of 0 to 50 μM.

We next explored the potential of the RES_{rep} device for cell/gene therapy, by stably integrating the RES_{rep} device driving SEAP into HEK293 cells. Although the device achieved success across a series of clonal cell lines, the best inhibition (~15.5-fold) was in a monoclonal $HEK_{RES\text{-}rep\text{-}SEAP}$ cell line (Fig. 1*C*). The $HEK_{RES\text{-}rep\text{-}SEAP}$ cell line showed excellent resveratrol dose- and time-dependent transgene expression (Fig. 1*D*). Moreover, this cell line exhibited sustained output over a 14-d culture (Fig. 1*E*) and displayed fully reversible transgene expression kinetics (Fig. 1*F*). For in vivo performance analysis of the resveratrol-controlled RES_{rep} device, $HEK_{RES\text{-}rep\text{-}SEAP}$ cells were microencapsulated in coherent alginate-poly-(l-lysine)-alginate beads and implanted into mice. After mice were given resveratrol (intraperitoneal [i.p.] injection, ranging from 0 to 500 mg/kg daily), we observed that SEAP production from the RES_{rep} device was controlled in a resveratrol dose-dependent manner (Fig. 1*G*) and observed sustained repression for 15 d in mice (Fig. 1*H*). These results confirm that RES_{rep} can precisely control transgene inhibition in mammalian cells and in mice.

Characterization of Resveratrol-Repressible CAR Expression (RES_{rep}-CAR) and CAR-Mediated T Cell Activity. Given previous studies reporting that resveratrol exerts potent antitumor effects against some cancers (46, 47) and may enhance human T cell activity (48, 49), we profiled the effects of resveratrol on the Jurkat T cells that we planned to use as the recipient cells for our devices to exclude any unanticipated impacts from the induction/repression agent (resveratrol). A total of 30 μM resveratrol had no significant effect on CAR expression or CD19 antigen-induced activation of unmodified Jurkat T cells (negative control) or conventional CAR-engineered Jurkat T cells (positive control; *SI Appendix*, Fig. S3).

We next developed a RES_{rep}-CAR device to inhibit CAR expression in engineered Jurkat T cells and primary T cells; this device was capable of selectively inactivating its therapeutic effects in the presence of resveratrol (Fig. 2*A*). First, we optimized the RES_{rep}-CAR device in Jurkat T cells ($Jurkat_{RES\text{-}rep\text{-}CAR}$) and found that a combination of P_{mPGK} (mouse phosphoglycerate kinase gene promoter)-driven $ResA_3$ and P_{ResA1}-driven CAR-P2A-EGFP achieved the best resveratrol-mediated performance in Jurkat T cells (*SI Appendix*, Fig. S4). These $Jurkat_{RES\text{-}rep\text{-}CAR}$ cells, which were transduced with the optimal RES_{rep}-CAR device, exhibited dose-dependent resveratrol-repressible CAR expression (Fig. 2*B*). These responses include CD69 expression (a general surface activation marker; Fig. 2*C*) and hIL-2 production (a general readout for effector T cell activation; Fig. 2*D*). Moreover, the RES_{rep}-CAR device enables fully reversible CAR expression in Jurkat T cells (Fig. 2*E*). We also found that the presence of resveratrol reduced the extent that the CD19 antigen stimulated the activation of the $Jurkat_{RES\text{-}rep\text{-}CAR}$. These results demonstrate that the RES_{rep} device can fine tune the repression of both CAR expression levels and the CAR-mediated cell activation of Jurkat T cells.

We subsequently optimized the RES_{rep}-CAR device in primary human T cells, which required the development of a particularly resveratrol-sensitive TtgR mutant (H67A) (50). The combination of P_{mPGK}-driven $ResA_4$ ($TtgR^{H67A}$-VPR) and P_{ResA1}-driven CAR exhibited excellent transgene inhibition upon incubation with 15 μM resveratrol in primary human T cells (*SI Appendix*, Fig. S5). These RES_{rep}-CAR T cells derived from primary human T cells exhibited titratable resveratrol-repressed CAR expression (Fig. 2*F*) as well as excellent CAR-regulated cell deactivation upon CD19 antigen stimulation in the presence of increased concentration of resveratrol, assessed via hIL-2 (Fig. 2*G*), and hIFN-γ (Fig. 2*H*) expression.

To test the cytotoxic performance of the engineered primary human T cells, we labeled $CD19^+$ K562 cells with mCherry ($CD19^+$ $K562_{mCherry}$) and $CD19^-$ K562 cells with EGFP ($CD19^-$ $K562_{EGFP}$) and then mixed them as a population of two target cell types that could be identified and measured by flow cytometry (*SI Appendix*, Fig. S6). The cytotoxic activity of the

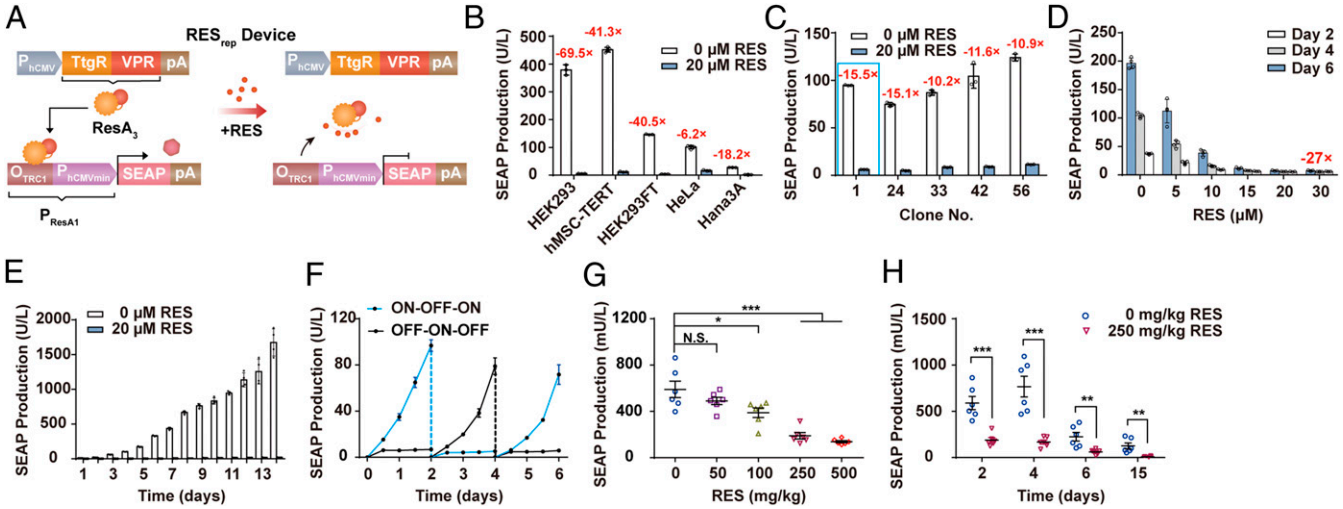

Fig. 1. Design and characterization of the resveratrol-repressible transgene expression device (RES$_{rep}$) in mammalian cells and mice. (*A*) Scheme for the RES$_{rep}$ device. The resveratrol-dependent transactivator ResA$_3$ (TtgR-VPR) module is formed by fusing a tripartite activator composed of VP64, p65, and Rta in tandem (VPR) to the C terminus of TtgR. In the absence of resveratrol, constitutively expressed ResA$_3$ binds a chimeric target promoter P$_{ResA1}$ (O$_{TRC1}$-P$_{hCMVmin}$) containing a tandem ResA$_3$-specific operator site O$_{TRC1}$ 5′ of a minimal human cytomegalovirus immediate-early promoter (P$_{hCMVmin}$), and activates SEAP production. The presence of resveratrol results in the release of ResA$_3$ from P$_{ResA1}$, thereby silencing SEAP production. (*B*) Resveratrol-repressible SEAP expression in different mammalian cell lines (HEK293, hMSC-TERT, HEK293FT, HeLa, or Hana3A) were cotransfected with pLF36 (P$_{hCMV}$-ResA$_3$-pA) and pLF31 (P$_{ResA1}$-SEAP-pA) and cultivated for 48 h in the presence or absence of resveratrol. (*C*) Selection of stably transgenic resveratrol-repressible cell lines (HEK-RES-rep-SEAP). HEK293 cells were cotransfected with pLF51 (ITR-O$_{TRC1}$-P$_{hCMVmin}$-SEAP-pA::P$_{hCMV}$-TtgR-VPR-P2A-PuroR-pA-ITR) and the transposase expression vector pCMV-T7-SB100 (P$_{hCMV}$-SB100X-pA). The selected cell clones were profiled for their resveratrol-repressible SEAP regulation performance. The blue frame marks the best-in-class clone chosen for the following experiments. (*D*) Resveratrol dose-dependent SEAP production in HEK$_{RES\text{-}rep\text{-}SEAP}$ cells. Different color bars represent different time periods for profiling SEAP production. (*E*) Long-term SEAP production kinetics of HEK$_{RES\text{-}rep\text{-}SEAP}$ stable cells. (*F*) Reversibility of HEK$_{RES\text{-}rep\text{-}SEAP}$-mediated SEAP production. HEK$_{RES\text{-}rep\text{-}SEAP}$ cells were cultivated for 6 d while altering resveratrol concentrations from 0 to 20 μM. Cell density was adjusted to 5×10^4 every 48 h, and SEAP production was profiled every 12 h. (*G*) Dose-dependent resveratrol-repressible SEAP production in mice. C57BL/6J mice implanted with 2×10^6 microencapsulated HEK$_{RES\text{-}rep\text{-}SEAP}$ cells were intraperitoneally injected with resveratrol once a day (0 to 500 mg/kg/d). SEAP production in blood was profiled after 48 h. (*H*) Long-term resveratrol-repressible SEAP production kinetics in mice. SEAP production was profiled at day 2, 4, 6, and 15. The data for *B*–*F* are mean ± SD, $n \geq 3$. The animal data of *G* and *H* are mean ± SEM. *P* values were calculated with Student's *t* test ($n = 6$ mice). $^*P < 0.05$; $^{**}P < 0.01$; $^{***}P < 0.001$ versus control. N.S., not statistically significant.

engineered primary T cells expressing CARs or the RES$_{rep}$-CARs were quantified as the selective reduction of CD19$^+$ K562$_{mCherry}$ cells. RES$_{rep}$-CAR T cells showed ~25% in vitro cytotoxic efficacy, tunable based on resveratrol concentration (Fig. 2*I*). Moreover, CAR-mediated T cell activation could be repressed by the RES$_{rep}$-CAR device in a time-dependent manner (*SI Appendix*, Fig. S7). Importantly, we confirmed that 15 μM resveratrol alone had no significant effects on either target cell lethality or cytokine production of non-RES$_{rep}$ regulated primary T cells modified with conventional CAR (*SI Appendix*, Fig. S8). In summary, we successfully constructed a RES$_{rep}$-CAR device for fine tuning CAR expression and applied it in Jurkat T cells and primary T cells.

Anticancer Performance of RES$_{rep}$-CAR T Cells in NCG Mice. To investigate whether the cytotoxic activity of RES$_{rep}$-CAR T cells could be regulated by resveratrol in mice, we evaluated target cell lethality and cytokine release in a rapid xenograft mouse tumor model of B cell leukemia (23) (Fig. 3). In this model, we implanted a mixture of CD19$^+$ K562$_{mCherry}$ and CD19$^-$ K562$_{EGFP}$ cells into the peritoneal cavity of NCG mice (NOD-*Prkdc*^{em26Cd52}*Il2rg*^{em26Cd22}/NjuCrl: triple immunodeficiency and lacking functional/mature T, B, and natural killer [NK] cells, along with reduced macrophage and dendritic cell function). After 10 h, we injected i.p. unmodified human primary T cells (negative control) or engineered human T cells equipped with RES$_{rep}$-CAR into the mice. Subsequently, we administered various doses of resveratrol (50, 100, or 200 mg/kg/d) or vehicle control by i.p. injection at the indicated times. Mice were killed after 48 h for peritoneal lavage collection, from which recovered cells were analyzed by flow cytometry; serum cytokine release analysis occurred at 24 h and 48 h (Fig. 3*A*).

Mice injected with RES$_{rep}$-CAR T cells showed resveratrol-repressible depletion of the CD19$^+$ K562$_{mCherry}$ cell population upon treatment with different resveratrol dosages; no depletion was observed for mice injected with control T cells (Fig. 3*B*). Further, comparison of the two dosages showed that serum cytokine levels (hIL-2 and hTNF) and extent of target cytotoxicity were tunable based on in vivo resveratrol concentration (Fig. 3 *C*–*G*). We confirmed that the high dosage of resveratrol (200 mg/kg/d) had no significant effect on the cytotoxicity capability in the positive control CAR T cells transplanted into mice (*SI Appendix*, Fig. S9). In summation, RES$_{rep}$-CAR T cells were able to achieve tunable cancer cell lethality in a mouse leukemia model.

Design, Construction, and Characterization of a RES$_{ind}$ Transgene Expression Device in Mammalian Cells and Mice. Our RES$_{rep}$-CAR T cells enable a strategy for negatively regulating T cell function, an attractive approach when the clinical response from a constitutively activated cell type requires inactivation; nevertheless, a RES$_{ind}$-CAR expression device should enable fine tuning therapeutic activity in a function-on manner. Pursuing this, we engineered a resveratrol-inducible on device (RES$_{ind}$) for controlling transgene expression in mammalian cells. Our designed RES$_{ind}$ device comprises a resveratrol-dependent transrepressor ResR$_1$ (TtgR-KRAB), based on fusing a Krüppel-associated box protein (KRAB) to the C terminus of TtgR; this can bind to the synthetic resveratrol-inducible promotor (P$_{ResR}$), harboring a constitutive expression promoter embedded with transrepressor ResR$_1$ binding sites (O$_{TRC1}$, a variant of O$_{TtgR}$), thereby repressing transgene expression. Resveratrol releases transrepressor ResR$_1$ from P$_{ResR}$ and induces transgene expression (Fig. 4*A*).

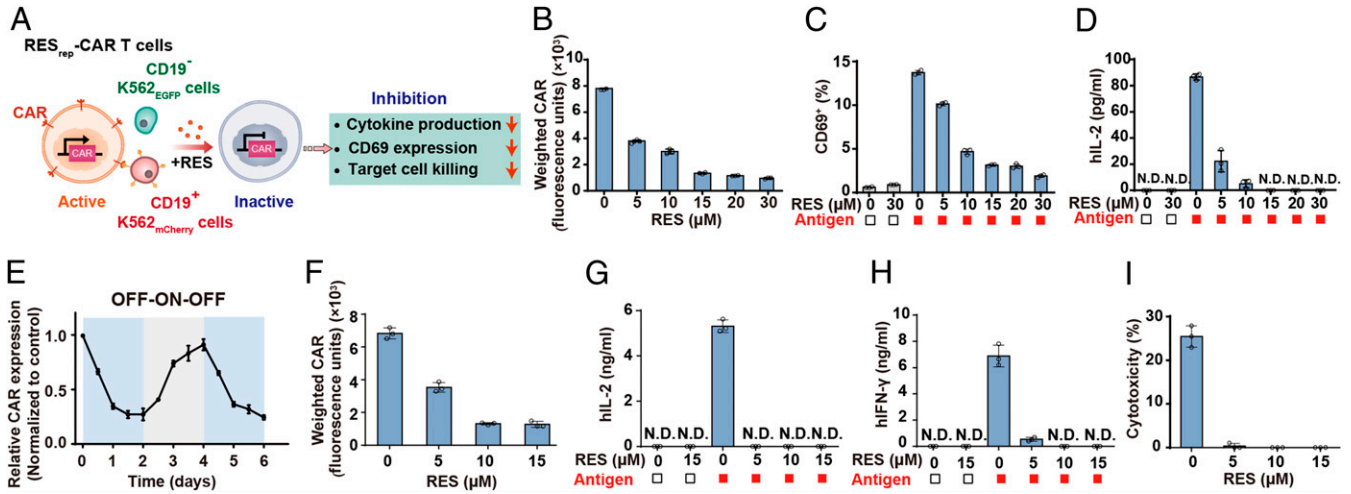

Fig. 2. Resveratrol-titratable T cell inactivation in Jurkat T and primary T cells engineered with RES$_{rep}$-CAR. (*A*) Scheme of the RES$_{rep}$-CAR device. Jurkat T cells or human primary T cells were modified utilizing lentivirus for resveratrol-repressible CAR expression. In the absence of resveratrol, RES$_{rep}$-CAR T cells exhibited sustained CAR expression, and these cells were activated upon antigen stimulation. In the presence of resveratrol, CAR expression was inhibited and the cells were insensitive to antigen stimulation. (*B*) Dose-dependent resveratrol-repressible CAR expression in Jurkat T cells (Jurkat$_{RES\text{-}rep\text{-}CAR}$). Jurkat T cells engineered with lentiviral pLF78 (LTR-P$_{mPGK}$-ResA$_3$-LTR) and pLF100 (LTR-P$_{ResA1}$-CAR-LTR) were cultivated in medium containing 0 to 30 μM resveratrol, and CAR expression was quantified by flow cytometry after 48 h. (*C* and *D*) Resveratrol and antigen-triggered Jurkat$_{RES\text{-}rep\text{-}CAR}$ cell activation. Cells were cultivated with various concentrations of resveratrol for 48 h and then incubated with CD19$^-$ K562$_{EGFP}$ cells (white squares) or CD19$^+$ K562$_{mCherry}$ cells (red squares) at an E:T ratio of 2:1. Surface expression of early T cell activation marker CD69 (*C*) and hIL-2 secretion (*D*), quantified after an overnight incubation. (*E*) Reversibility of RES$_{rep}$-CAR device-mediated CAR expression in Jurkat T cells. Cells transduced with lentiviral pLF363 (LTR-P$_{mPGK}$-ResA$_4$-LTR) and pLF100 were cultivated without (gray rectangles) or with 20 μM resveratrol (blue rectangles). The relative mRNA level of CAR was quantified by qPCR every 12 h and normalized to the control group incubated without resveratrol. Cell density was adjusted to 1×10^6 cells/mL every 48 h. (*F*) Dose-dependent resveratrol-repressible CAR surface expression in human primary T cells (RES$_{rep}$-CAR T cells). RES$_{rep}$-CAR T cells engineered with optimized the RES$_{rep}$-CAR device were transduced with lentiviral pLF363 and pLF100, and then cells were cultivated in medium containing 0 to 15 μM resveratrol. CAR expression was quantified by flow cytometry after 48 h. (*G* and *H*) RES$_{rep}$-CAR T cell-mediated cytokine release. RES$_{rep}$-CAR T cells were cultivated with various concentrations of resveratrol for 48 h and then incubated with CD19$^-$ K562$_{EGFP}$ cells (white squares) or CD19$^+$ K562$_{mCherry}$ cells (red squares) at an E:T ratio of 5:1. hIL-2 (*G*) and hIFN-γ (*H*) were quantified after 18-h incubation. (*I*) RES$_{rep}$-CAR T cell-mediated targeted cytotoxicity. RES$_{rep}$-CAR T cells were cultivated with various concentrations of resveratrol for 48 h and then incubated with a mixture of target cells containing CD19$^-$ K562$_{EGFP}$ cells and CD19$^+$ K562$_{mCherry}$ cells at an E:T ratio of 10:1. After 18 h, cells were collected for flow cytometry analysis and cytotoxicity values were calculated based on the ratios of CD19$^+$ K562$_{mCherry}$ cells to CD19$^-$ K562$_{EGFP}$ cells. The data in *B*–*I* are mean ± SD, $n = 3$. N.D., not detectable.

To obtain the envisioned RES$_{ind}$ device with minimal leakage in the absence of resveratrol and strong resveratrol-induced transgene expression, we optimized the RES$_{ind}$ device by testing different O$_{TtgR}$ variants, different variants of resveratrol-responsive promoters, and different strengths of constitutive promoters for driving TtgR expression (*SI Appendix*, Figs. S10 and S11). Due to its superior induction performance, the variant O$_{TRC1}$ (reverse complement and site-directional mutation of O$_{TtgR}$) was initially chosen as the optimal binding sequence for the subsequent optimization of resveratrol-responsive promoters. Ultimately, we determined that a combination of P$_{hCMV}$-drived TtgR with the resveratrol-responsive promoter P$_{ResR12}$ [O$_{TRC1}$-P$_{hCMV}$-(O$_{TRC1}$)$_2$] exhibited optimal induction performance in HEK293 cells (*SI Appendix*, Fig. S11*O*), and this version of the RES$_{ind}$ device also achieved significant induction performance across five human cell lines (Fig. 4*B*) and strong time-course–dependent performance (*SI Appendix*, Fig. S12).

As in our characterization of the RES$_{rep}$ device in assessing suitability for cell/gene therapy, we evaluated the best monoclonal HEK$_{RES\text{-}ind\text{-}SEAP}$ cell line (378-fold induction; Fig. 4*C*), from the examined clones and found that it showed excellent resveratrol dose- and time-dependent transgene expression (Fig. 4*D*). Moreover, this cell line exhibited sustained resveratrol-induced transgene output throughout a 14-d culture (Fig. 4*E*) and fully resveratrol-reversible transgene expression kinetics (Fig. 4*F*).

We then microencapsulated HEK$_{RES\text{-}ind\text{-}SEAP}$ cells and implanted them into mice to assess resveratrol-induced in vivo transgene expression from the RES$_{ind}$ device. After mice were intraperitoneally administrated with resveratrol at doses ranging from 0 to 250 mg/kg daily, we observed that resveratrol could control SEAP production in a dose-dependent manner (Fig. 4*G*), over an induction window of 15 d (Fig. 4*H*). These results confirm that the RES$_{ind}$ device can fine tune transgene induction in mammalian cells and in mice.

Seeking to decrease the amount of RES needed to trigger the RES$_{ind}$ device, and ultimately aiming to achieve controlled transgene expression based on the oral administration of resveratrol, we attempted to further improve the sensitivity of our RES$_{ind}$ device by testing various mutants of the TtgR protein (*SI Appendix*, Fig. S13). The RES$_{ind\text{-}mut}$ device proved to be substantially more sensitive to resveratrol than our initial device. The combination of P$_{hCMV}$-driven ResR$_4$ (TtgR^{H67A}-KRAB) and P$_{ResR12}$-driven SEAP exhibited the best induction performance in HEK293 cells with dose- and time-course–dependent induction kinetics, especially at lower resveratrol concentrations (0 to 5 μM; *SI Appendix*, Fig. S13 *A* and *B*). We next constructed and selected a highly sensitive and inducible isogenic cell clone that allowed for the RES-inducible transgene expression of SEAP (HEK$_{RES\text{-}ind\text{-}mut\text{-}SEAP}$). The RES$_{ind\text{-}mus}$ device continued to show superior transgene induction at low resveratrol concentrations (0 to 6 μM; *SI Appendix*, Fig. S13*C*). When the microencapsulated HEK$_{RES\text{-}ind\text{-}mut\text{-}SEAP}$ cells were implanted into mice, regardless of delivery method (intraperitoneal injection or oral intake of resveratrol), resveratrol controlled transgene expression in a dose-dependent manner (*SI Appendix*, Fig. S13 *D*–*G*). These results demonstrate that the RES$_{ind\text{-}mus}$ device is successful in being more sensitive to resveratrol.

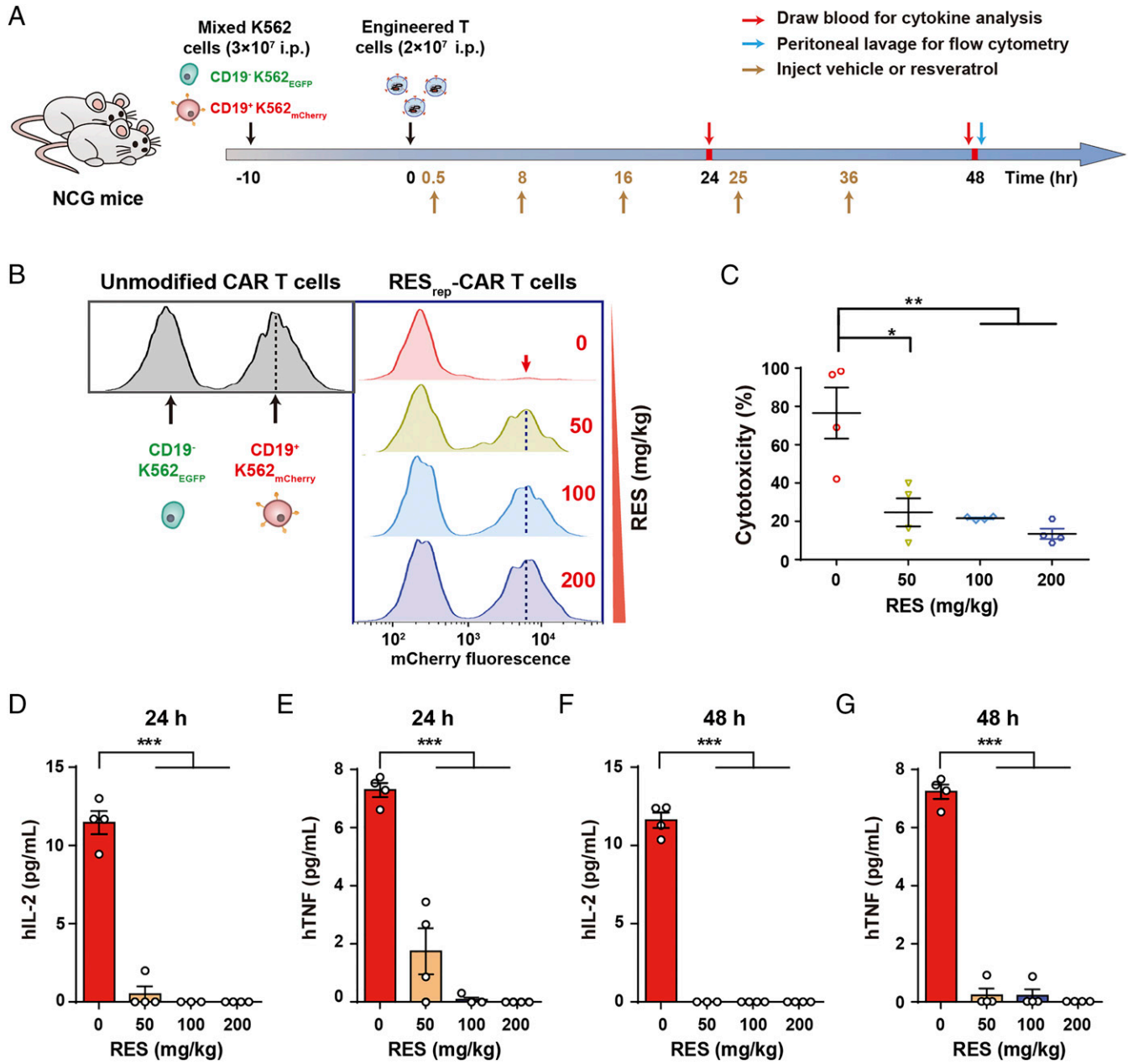

Fig. 3. Resveratrol-repressible activation of primary human T cells engineered with RES_{rep}-CAR in NCG mice. (*A*) Experimental design for in vivo assessment of resveratrol-controlled RES_{rep}-CAR T cell-mediated cytotoxicity against K562 cells in a rapid xenograft mouse tumor model. NCG mice inoculated with 3×10^7 mixed K562 cells ($CD19^-$ $K562_{EGFP}$ cells:$CD19^+$ $K562_{mCherry}$ cells = 1:1) were injected intraperitoneally with 2×10^7 unmodified primary human T cells (control) or RES_{rep}-CAR T cells, followed by the administration of various resveratrol doses (50, 100, or 200 mg/kg/d) or vehicle control at the indicated times. After 48 h, blood was drawn for cytokine examination and peritoneal cells were quantified by flow cytometry to measure in vivo cytotoxicity. (*B*) Representative flow cytometry data show the resveratrol-repressible depletion of the $CD19^+$ $K562_{mCherry}$ cell population. (*C*) Quantified target cytotoxicity results for all experimental groups. Cytotoxicity values were calculated from the ratios of $CD19^+$ $K562_{mCherry}$ cells to $CD19^-$ $K562_{EGFP}$ cells. $n = 4$ mice. (*D–G*) In vivo hIL-2 (*D* and *F*) and hTNF (*E* and *G*) release at 24 h and 48 h. The data in *C–G* are mean ± SEM. *P* values were calculated with Student's *t* test ($n = 4$ mice). $^*P < 0.05$; $^{**}P < 0.01$; $^{***}P < 0.001$ versus control.

Tunability and Kinetics of RES_{ind}-CAR Expression in Jurkat T Cells. We next developed a RES_{ind}-CAR expression device to positively regulate CAR expression in engineered Jurkat T cells and primary T cells; this device was capable of selectively activating therapeutic effects in the presence of resveratrol and upon CD19 antigen stimulation (Fig. 5*A*).

To characterize the performance of the RES_{ind}-CAR device in T cells and obtain an optimal RES_{ind}-CAR device, with low transgene expression leakage in the absence of resveratrol and high induction rates in the presence of resveratrol, we used the RES_{ind}-CAR device to control the transcriptional activation of a transgene cassette, comprising both enhanced green fluorescent protein (EGFP) and CAR, and optimized the resveratrol-inducible CAR-P2A-EGFP expression device in Jurkat T cells ($Jurkat_{RES\text{-}ind\text{-}CAR\text{-}EGFP}$) by measuring the EGFP expression level. Guided by a previous study (51), we optimized the resveratrol-inducible promotor and the constitutive promoters for driving $ResR_1$ expression with P_{mPGK} and $P_{hEF1\alpha}$ (human extension factor

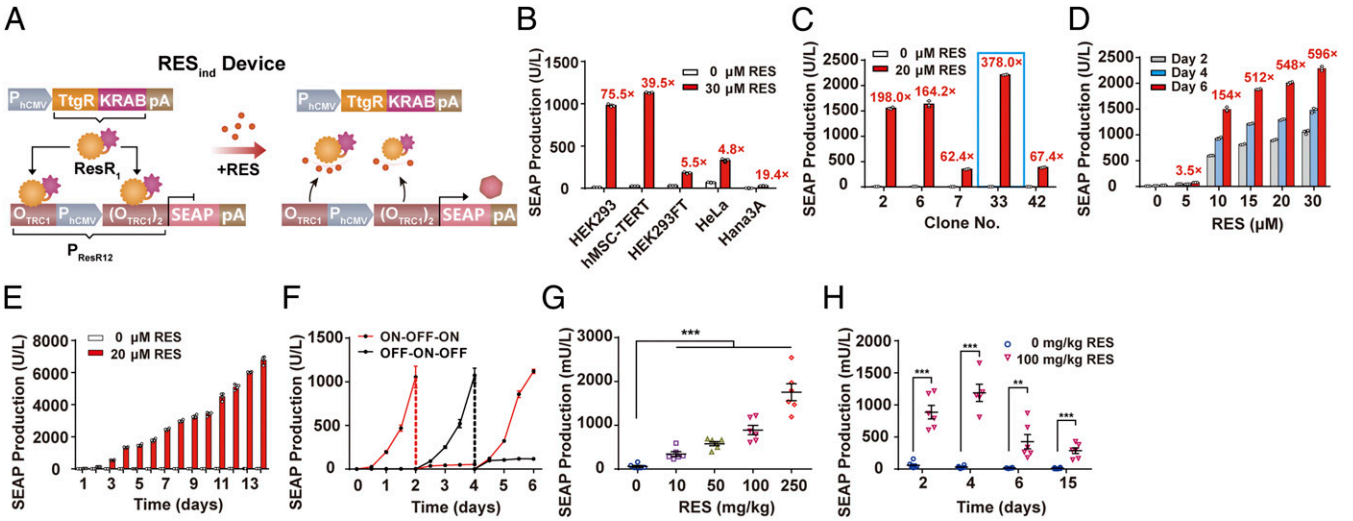

Fig. 4. Design and characterization of a resveratrol-inducible transgene expression device (RES_{ind}) in mammalian cells and mice. (*A*) Schematic showing RES_{ind} device design and the experimental procedure for resveratrol-controlled transgene expression assessment in mice. TtgR was fused to a transsilencing human Krüeppel-associated box (KRAB) domain to obtain the resveratrol-dependent transrepressor $ResR_1$ (TtgR-KRAB), which is driven by the human cytomegalovirus immediate early promoter P_{hCMV}. In the absence of resveratrol, $ResR_1$ binds to a chimeric target promoter P_{ResR12} [O_{TRC1}-P_{hCMV}-$(O_{TRC1})_2$], containing the $ResR_1$-specific DNA binding site O_{TRC1} positioned at the 3′ and 5′ ends of P_{hCMV}; this represses P_{hCMV}-driven SEAP production. In the presence of resveratrol, $ResR_1$ is released from P_{ResR12} and initiates SEAP production. (*B*) Resveratrol-inducible SEAP production in various mammalian cell lines. HEK293, hMSC-TERT, HEK293FT, HeLa, and Hana3A cells cotransfected with pLF25 (P_{hCMV}-$ResR_1$-pA) and pLF18 (P_{ResR12}-SEAP-pA) were cultivated for 48 h in the presence or absence of 20 μM resveratrol. (*C*) Selection of stably transgenic resveratrol-inducible cell lines ($HEK_{RES\text{-}ind\text{-}SEAP}$). HEK293 cells were cotransfected with pLF50 (ITR-P_{ResR12}-SEAP-pA::P_{hCMV}-TtgR-KRAB-P2A-PuroR-pA-ITR) and the transposase expression vector pCMV-T7-SB100 (P_{hCMV}-SB100X-pA). The selected cell clones were profiled for their resveratrol-inducible SEAP regulation performance. The blue frame marks the best-in-class clone chosen for the following experiments. (*D*) Resveratrol dose-dependent SEAP production in $HEK_{RES\text{-}ind\text{-}SEAP}$ cells. Different color bars represent different time periods for profiling SEAP production. (*E*) Long-term SEAP production kinetics in $HEK_{RES\text{-}ind\text{-}SEAP}$ stable cells. (*F*) Reversibility of $HEK_{RES\text{-}ind\text{-}SEAP}$-mediated SEAP production. $HEK_{RES\text{-}ind\text{-}SEAP}$ cells were cultivated for 6 d while altering the resveratrol concentrations from 0 to 20 μM. Cell density was adjusted to 5×10^4 every 48 h and SEAP production was profiled every 12 h. (*G*) Dose-dependent resveratrol-inducible SEAP production in mice. C57BL/6J mice implanted with 2×10^6 microencapsulated $HEK_{RES\text{-}ind\text{-}SEAP}$ cells were intraperitoneally injected with resveratrol once a day (0 to 250 mg/kg/d). SEAP production in blood was profiled after 48 h. (*H*) Long-term resveratrol-inducible SEAP production kinetics in mice. SEAP production was profiled on days 2, 4, 6, and 15. The data in *B*–*F* are mean ± SD, $n \geq 3$ independent experiments. The animal data *G* and *H* are mean ± SEM. *P* values were calculated with Student's *t* test ($n = 6$ mice). $^{**}P < 0.01$; $^{***}P < 0.001$ versus control.

α gene promoter). We found that a combination of P_{mPGK}-driven $ResR_1$ and P_{ResR11} [O_{TRC1}-P_{hEF1a}-$(O_{TRC1})_2$]–driven CAR-P2A-EGFP showed the best induction performance in Jurkat T cells (*SI Appendix*, Fig. S14).

$Jurkat_{RES\text{-}ind\text{-}CAR\text{-}EGFP}$ cells, which were transduced with the optimal RES_{ind}-CAR-EGFP device, exhibited excellent resveratrol dose-dependent control of CAR and EGFP expression, with extremely strong transgene induction at a low (15 μM) resveratrol concentration (Fig. 5*B*). Moreover, by observing changes in EGFP expression via flow cytometry, we found that $Jurkat_{RES\text{-}ind\text{-}CAR\text{-}EGFP}$ cells possessed excellent long-time induction performance with negligible leakage and nonsaturating increases in EGFP expression over 14 d (Fig. 5*C* and *SI Appendix*, Fig. S15). Moreover, experiments in which we periodically added then removed resveratrol demonstrated that the device enables fully reversible transgene expression (Fig. 5 *D* and *E* and *SI Appendix*, Fig. S16). We also verified that the induced $Jurkat_{RES\text{-}ind\text{-}CAR\text{-}EGFP}$ cells, which express CAR in a resveratrol dose-dependent manner, could be activated by CD19-positive K562 cells ($CD19^+$ $K562_{mCherry}$), as assessed by CD69 induction (Fig. 5*F*) and hIL-2 production (Fig. 5*G*). We also observed that the RES_{ind}-CAR device showed CD19 antigen density-dependent response in Jurkat T cells (*SI Appendix*, Fig. S17). These results demonstrate that the RES_{ind} device can fine tune CAR expression and CAR-mediated cell activation in Jurkat T cells.

Resveratrol-Inducible CAR Expression in Primary Human T Cells. Next, we further optimized the RES_{ind}-CAR device in primary human T cells with different configurations of resveratrol-inducible promotors and various mutants of the TtgR protein (*SI Appendix*, Figs. S18 and S19) guided by data from previously reported studies (44, 50, 52). A combination of $P_{hEF1\alpha}$-driven $ResR_4$ ($TtgR^{H67A}$-KRAB) and P_{ResR15} (O_{TRC1}-P_{hEF1a}-O_{TRC1})–driven CAR showed the best induction performance and was used for further studies in primary T cells.

Primary T cells engineered with the optimized RES_{ind}-CAR device exhibited titratable CAR expression controlled by resveratrol (Fig. 5*H*) and resveratrol-controlled CAR-related cell activation upon antigen stimulation, as assessed by hIL-2 production (Fig. 5*I*) and hIFN-γ production (Fig. 5*J*). Cytotoxicity assays demonstrated that the cytotoxic efficacy of RES_{ind}-CAR T cells against $CD19^+$ $K562_{mCherry}$ is excellent and is tunable on resveratrol dosage (Fig. 5*K*). Moreover, CAR-induced T cell activation can be mediated by the RES_{ind}-CAR device in a time-dependent manner as well (*SI Appendix*, Fig. S20). In summary, we generated a RES_{ind}-CAR device to control transgene induction, CAR T cell activation, and cancer cell lethality in T cells.

Resveratrol-Controlled Cancer Cell Lethality Mediated by RES_{ind}-CAR T Cells in NCG Mice. To evaluate antitumor efficacy mediated by the RES_{ind}-CAR device in vivo, we established two xenograft tumor mouse models. We first investigated whether the activity of RES_{ind}-CAR T cells could be regulated by resveratrol in a dose-dependent manner in a rapid xenograft mouse model of B cell leukemia (Fig. 6). In this model, unmodified T cells (Ctrl) or RES_{ind}-CAR T cells were injected i.p. after NCG mice were implanted with a mixture of $CD19^+$ $K562_{mCherry}$ and $CD19^-$ $K562_{EGFP}$ cells. These mice were then administrated with various

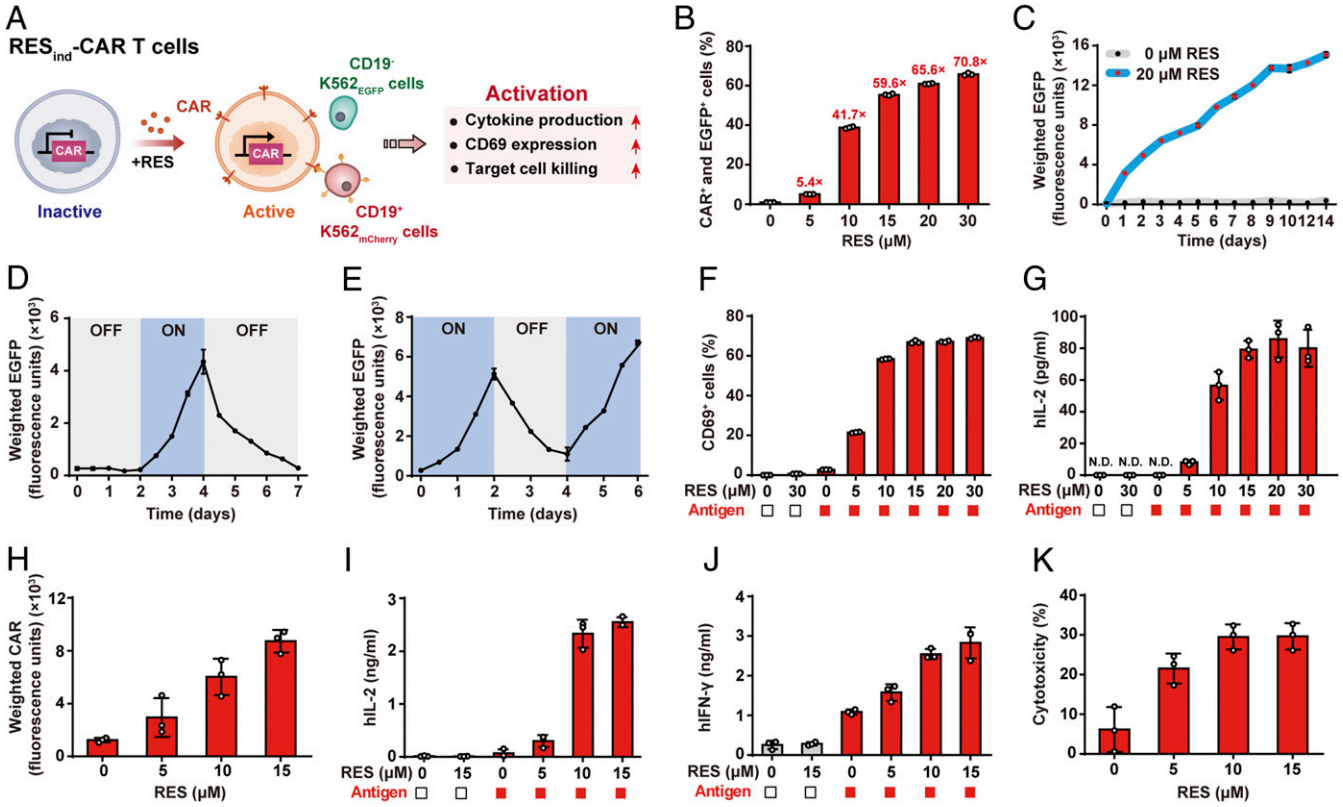

Fig. 5. Resveratrol-titratable activation of Jurkat T and primary T cells engineered with RES$_{ind}$-CAR. (*A*) Schematic of the RES$_{ind}$-CAR device. Jurkat T cells or human primary T cells were engineered with lentivirus to express RES$_{ind}$-CAR. In the absence of resveratrol, CAR expression was repressed and T cells were insensitive to antigen-mediated activation. The presence of resveratrol induced CAR expression, and these CAR$^+$ T cells were activated by antigen-positive (CD19$^+$) K562 target cells (assessed based on cytokine production, CD69 expression, and cell killing assays). (*B*) Dose-dependent resveratrol-inducible CAR and EGFP expression in Jurkat T cells (Jurkat$_{RES\text{-}ind\text{-}CAR\text{-}EGFP}$). Jurkat$_{RES\text{-}ind\text{-}CAR\text{-}EGFP}$ cells engineered with lentiviral pLF63 (LTR-P$_{mPGK}$- ResR$_1$-LTR) and pLF64 (LTR-P$_{ResR11}$-CAR-P2A-EGFP-LTR) were cultivated with different concentrations of resveratrol for 48 h. Expression levels of CAR and EGFP were quantified by flow cytometry. (*C*) Long-term Jurkat$_{RES\text{-}ind\text{-}CAR\text{-}EGFP}$-mediated EGFP expression. (*D* and *E*) Reversibility of Jurkat$_{RES\text{-}ind\text{-}CAR\text{-}EGFP}$-mediated EGFP expression. Cells were cultivated without (gray rectangles) or with 20 μM resveratrol (blue rectangles) periodically; EGFP expression was profiled every 12 h. Cell density was adjusted to 1×10^6 cells/mL every 48 h. (*F* and *G*) Resveratrol and antigen-triggered Jurkat$_{RES\text{-}ind\text{-}CAR\text{-}EGFP}$ cell activation. Cells were cultivated with various concentrations of resveratrol for 48 h and then incubated with CD19$^-$ K562$_{EGFP}$ cells (white squares) or CD19$^+$ K562$_{mCherry}$ cells (red squares) at an E:T ratio of 2:1. After overnight incubation, the surface expression of the T cell activation markers CD69 (*F*) and hIL-2 secretion (*G*) were quantified. (*H*) Dose-dependent CAR surface expression of the optimized RES$_{ind}$-CAR device in human primary T cells (RES$_{ind}$-CAR T cells). RES$_{ind}$-CAR T cells engineered with lentiviral pLF355 (LTR-P$_{ResR15}$-CAR-LTR) and pLF361 (LTR-P$_{mPGK}$-ResR$_4$-LTR) were cultivated in medium containing 0 to 15 μM resveratrol, and CAR expression was quantified by flow cytometry after 48 h. (*I* and *J*) Resveratrol-controlled cytokine release from RES$_{ind}$-CAR T cells. RES$_{ind}$-CAR T cells were cultivated with various concentrations of resveratrol for 48 h and then incubated with CD19$^-$ K562$_{EGFP}$ cells (white squares) or CD19$^+$ K562$_{mCherry}$ cells (red squares) at an E:T ratio of 5:1. hIL-2 (*I*) and hIFN-γ (*J*) production were quantified after overnight incubation. (*K*) Resveratrol-inducible target cytotoxicity of RES$_{ind}$-CAR T cells. Cells were cultivated with various concentrations of resveratrol for 48 h and then incubated with a mixture of target cells containing CD19$^-$ K562$_{EGFP}$ cells and CD19$^+$ K562$_{mCherry}$ cells at an E:T ratio of 10:1. After 18 h, cells were collected for flow cytometry and cytotoxicity values were calculated based on ratios of CD19$^+$ K562$_{mCherry}$ cells to CD19$^-$ K562$_{EGFP}$ cells. The data in *B*–*K* are mean ± SD, $n = 3$. N.D., not detectable.

doses of resveratrol (5 to 100 mg/kg/d) or vehicle control. Serum cytokine release was analyzed every 24 h and the cytotoxicity of RES$_{ind}$-CAR T cells was quantified by flow cytometry at 48 h (Fig. 6*A*). Mice injected with RES$_{ind}$-CAR T cells showed resveratrol-dependent depletion of the CD19$^+$ K562$_{mCherry}$ cell population (Fig. 6*B*). RES$_{ind}$-CAR T cells killed target cells in a resveratrol-inducible manner, with the strongest cytotoxicity observed with a resveratrol dosage of 10 mg/kg/d (Fig. 6*C*). Consistently, monitoring in vivo hIL-2 and hTNF cytokine release demonstrated that the activity of RES$_{ind}$-CAR T cells was tunable to the resveratrol concentration (Fig. 6 *D*–*G*).

We further assessed antitumor efficacy mediated by RES$_{ind}$-CAR T cells in an aggressive leukemia xenograft model in NSG mice (Fig. 7). We engrafted mice with Renilla luciferase (Rluc)–expressing CD19$^+$ K562 cells intravenously. After 5 d, mice received control unmodified T cells (Ctrl), conventional CAR T cells (Conv. CAR), or RES$_{ind}$-CAR T cells intravenously, followed by daily intraperitoneal (50 mg/kg) or oral (250 mg/kg) resveratrol (Fig. 7*A*). Serum cytokines were quantified after T cell infusion on day 3 and significant secretion of hIL-2 and hTNF was found in mice infused with RES$_{ind}$-CAR T cells and resveratrol (Fig. 7 *B* and *C*). Additionally, tumor burden was demonstrated by bioluminescence imaging, and the results demonstrated that tumor growth was significantly suppressed in mice that received RES$_{ind}$-CAR T cells with resveratrol treatment for 28 d (Fig. 7 *D*–*F*). A similar suppression was seen in mice that received conventional CAR T cells. The observed tumor flux in mice that received the RES$_{ind}$-CAR T cells in the presence of resveratrol was significantly lower than those that received the RES$_{ind}$-CAR T cells in the absence of resveratrol (Fig. 7*F*). In contrast, tumor flux in mice that received RES$_{ind}$-CAR T cells in the absence of resveratrol increased similarly to mice that received unmodified T cells. Furthermore, we observed prolonged survival in mice infused with RES$_{ind}$-CAR T cells and resveratrol (Fig. 7*G*).

Collectively, these results demonstrate that the cytotoxic activity of RES$_{ind}$-CAR T cells against tumor cells can be fine

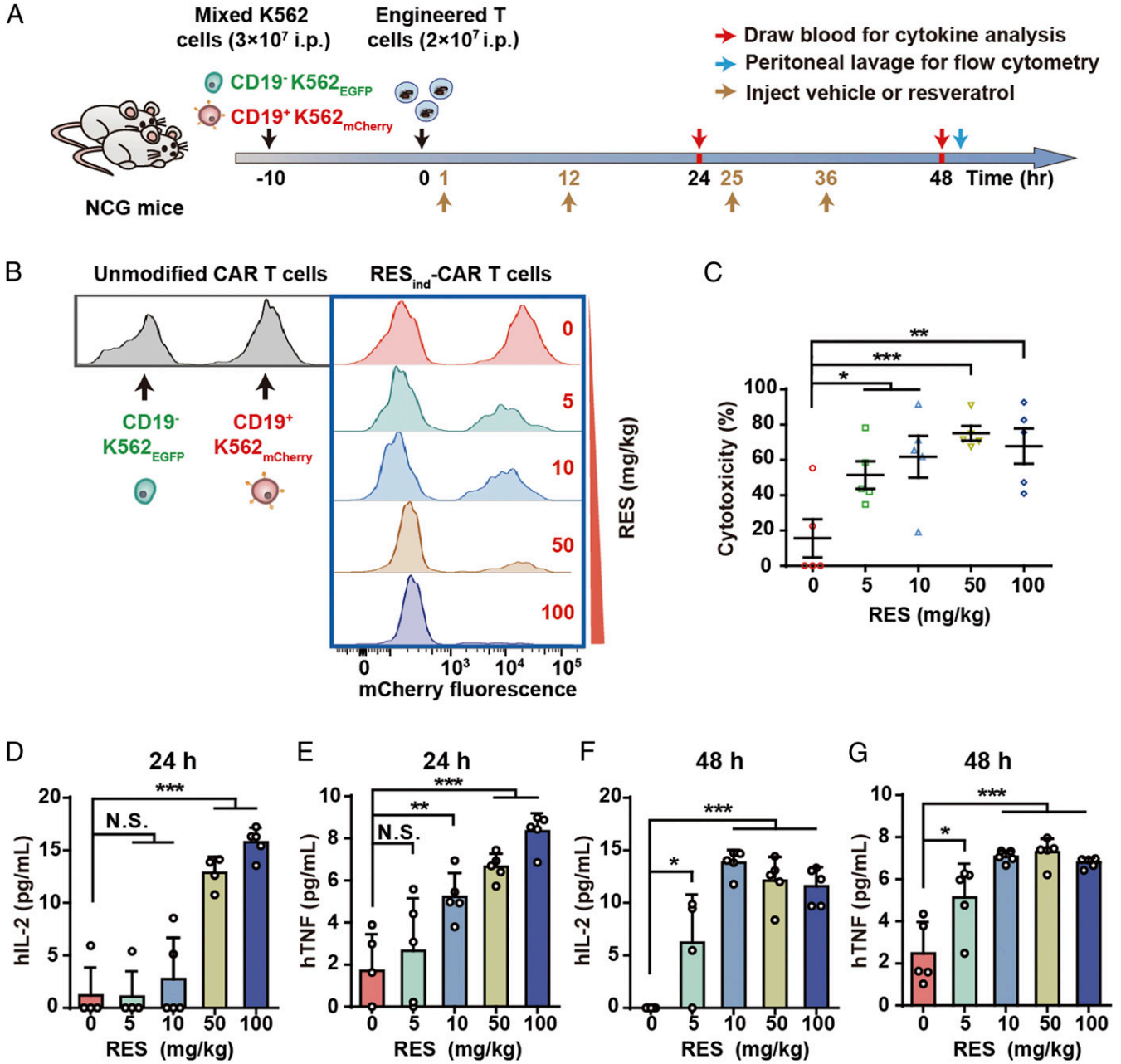

Fig. 6. Targeted cytotoxicity by primary human T cells engineered with RES_{ind}-CAR in NCG mice. (*A*) Experimental design for in vivo assessment of resveratrol-inducible cancer cell lethality by RES_{ind}-CAR T cells in a rapid xenograft tumor mouse model. NCG mice inoculated with $CD19^{-}$ $K562_{EGFP}$ cells and $CD19^{+}$ $K562_{mCherry}$ cells were injected intraperitoneally with 2×10^7 unmodified primary human T cells (control) or RES_{ind}-CAR T cells and then administered with resveratrol or vehicle control at the indicated times. After 48 h, blood was drawn for cytokine analysis and peritoneal cells were quantified by flow cytometry to measure in vivo cytotoxicity. (*B*) Representative flow cytometry data show the resveratrol-inducible depletion of the $CD19^{+}$ $K562_{mCherry}$ cell population. (*C*) Quantified flow cytometry results of targeted cytotoxicity by RES_{ind}-CAR T cells. (*D*–*G*) In vivo hIL-2 (*D* and *F*) and hTNF (*E* and *G*) release of RES_{ind}-CAR T cells controlled by resveratrol at 24 h and 48 h. The data in *B*–*G* are mean ± SEM. *P* values were calculated with Student's *t* test ($n = 4$ to 5 mice). $^{*}P < 0.05$; $^{**}P < 0.01$; $^{***}P < 0.001$ versus control. N.S., not statistically significant.

tuned by resveratrol in mice, suggesting potential applications for controlling CAR T cell activity in patients.

Discussion

Here, we report the development of resveratrol-controlled transgene expression devices (RES_{rep} and RES_{ind}) based on the TtgR regulatory device to preciously control transgene expression in mammalian cells and mice. We further demonstrate that the RES_{rep} and RES_{ind} devices are effective in controlling CAR expression in T cells to guide the recognition and eradication of tumor cells, both in vitro and in vivo. These resveratrol-controlled devices establish a proof of concept for cancer immunotherapy strategies based on the resveratrol-regulated repression or induction of immune cells.

In recent years, synthetic biology-inspired therapeutic programs have achieved favorable outcomes in the treatment of various diseases, including diabetes (53–55), insulin resistance (56), liver disorders (57), bacterial infections (58), and cancer (59–62); several of these treatments require effective, long-term therapeutic outputs, achieved by the sustained delivery of trigger

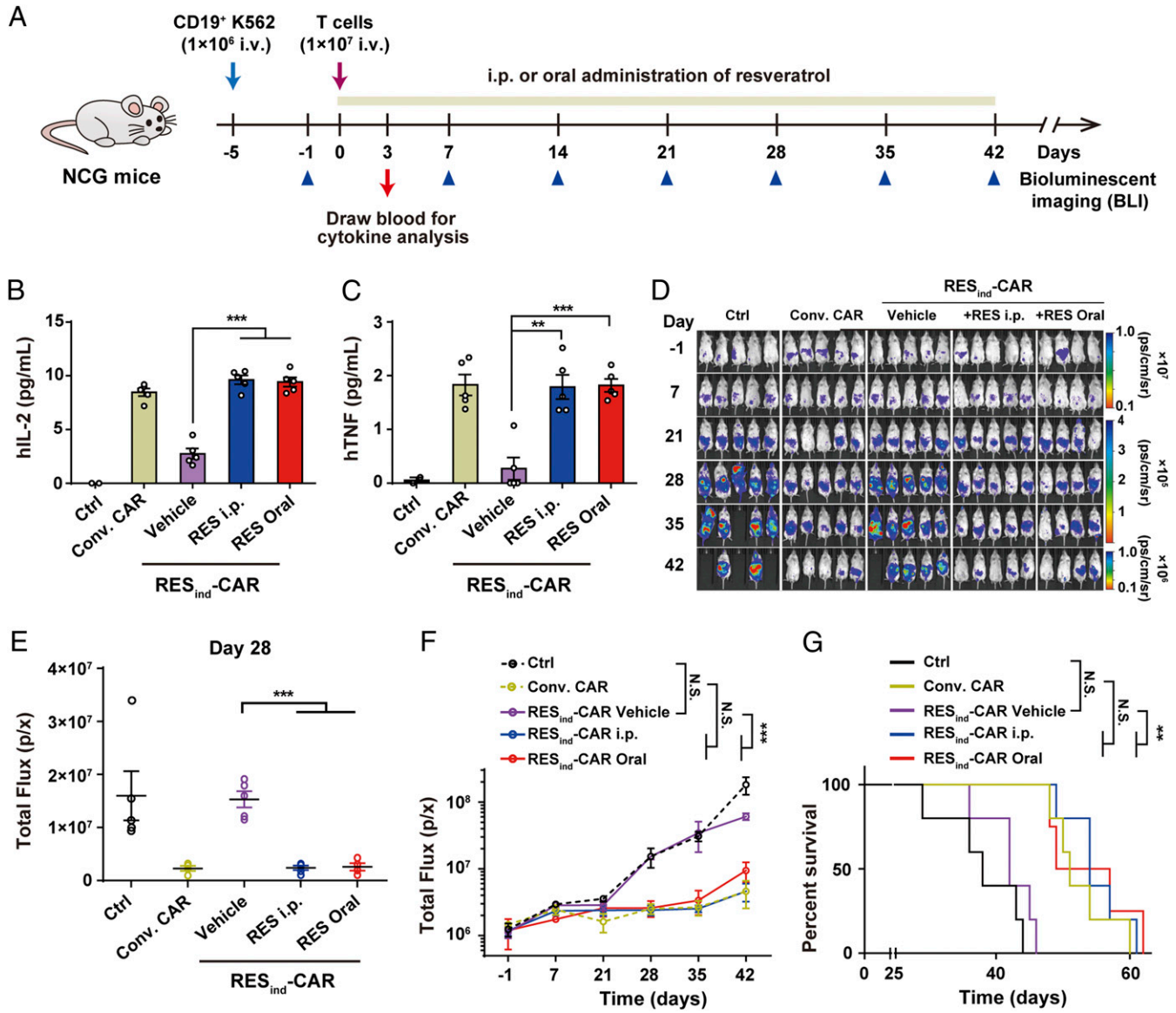

Fig. 7. In vivo efficacy of RES$_{ind}$-CAR T cells in CD19$^+$ K562 xenograft mouse models. (*A*) Experimental design for xenograft mouse model in vivo studies. NSG mice were injected intravenously (i.v.) with Rluc-expressing CD19$^+$ K562 cells (1×10^6). After 6 d, mice were infused with unmodified T cells (Ctrl), conventional CAR T cells (Conv. CAR), or resveratrol-inducible CAR expression T cells (RES$_{ind}$-CAR), followed by daily intraperitoneal (50 mg/kg) or oral (250 mg/kg) administration of resveratrol. (*B* and *C*) Human cytokine hIL-2 (*B*) and hTNF (*C*) were measured at 3 d after T cell infusion. (*D*) Tumor burden images obtained by BLI of groups treated with: unmodified T cells (Ctrl), conventional CAR T cells (Conv. CAR), RES$_{ind}$-CAR without resveratrol, RES$_{ind}$-CAR with resveratrol by injection, and RES$_{ind}$-CAR with resveratrol by oral administration at different days as indicated. (*E*) Quantification of tumor burden on day 28 was plotted based on BLI total flux (photons per second) of each mouse shown in *D* using IVIS imaging. (*F*) The tumor burden of each group was monitored for up to 42 d after T cell infusion. Tumor burden was quantified as the total flux from the Rluc activity of each mouse using IVIS imaging. The data in *B*, *C*, *E*, and *F* are mean ± SEM. *P* values were calculated with Student's *t* test ($n = 4$ to 5 mice). $^{**}P < 0.01$; $^{***}P < 0.001$ versus control. (*G*) Kaplan–Meier curve representing the survival percentage of the experimental groups. *P* values were determined using two-sided log-rank test. N.S., not statistically significant.

molecules. The natural dietary molecule resveratrol, an antioxidant in red wine, has been a part of the human diet for thousands of years and is generally recognized as safe; resveratrol has already seen use in cosmetics and some healthcare products. This study demonstrates that RES$_{ind}$ and RES$_{rep}$ devices can achieve titratable, reversible, and long-term control of low concentration resveratrol-regulated transgene expression in mammalian cells and mice.

CAR T cell therapy is a paradigm-shifting therapeutic approach for cancer treatment that is achieving tremendous success in the clinic; however, its increasing utilization is revealing many unpredictable and/or uncontrollable side effects from on-target/off-tumor toxicity, including severe CRS (sCRS) and neurotoxicity (13), tumor lysis syndrome, and the eradication of normal cell types expressing low levels of an antigen (63). Our RES$_{rep}$-CAR expression device can be used to block the activity of infused CAR T cells, potentially being deployed to prevent toxicity-associated morbidity and mortality when patients are considered at a high risk for clinical complications in early-stage CAR T therapy. We verified that T cells engineered with RES$_{rep}$-CAR provide effective and titratable inhibition over T cell activation, while retaining their inducible therapeutic efficacy upon resveratrol removal. The pattern and extent of functional inhibition achieved by resveratrol in our study highlights the clinical potential of RES$_{rep}$-CAR.

We envision the RES$_{ind}$-CAR device to be implemented with patients who are in danger of developing severe responses to cell

infusion. Our results demonstrate that T cells engineered with RES_{ind}-CAR can fine tune CAR expression levels and associated CAR-mediated cell activation, in vitro and in vivo, by adjusting administered resveratrol concentrations. In practice, the use of RES_{ind}-CAR in clinical trials could be coincident with monitoring cell infusion toxicity responses and real-time CAR T cells efficacy, enabling ongoing resveratrol-mediated CAR T cell activity adjustment to achieve highly precise, personalized, therapeutic outcomes.

Despite the excellent regulation performance of resveratrol-controlled transgene expression devices in vitro and in vivo, there is still room for improvement from a translational perspective. For example, given the low bioavailability of resveratrol by oral administration, the response sensitivity of resveratrol-controlled devices will require further engineering and optimization. We anticipate that more sensitive devices could be obtained by optimizing the operator sequences and directed evolution approaches, or via rational protein design to alter the transactivator and/or transrepressor properties. Furthermore, combination with our previously engineered and orthogonal systems (53) could enable multilayered control and even safer therapies.

With its broad potential uses, promising therapeutic impact for numerous diseases, and nutraceutical properties, resveratrol is a particularly suitable trigger molecule for clinical applications. Our work shows that resveratrol-controlled genetic devices can expand the toolbox of cybergenetics and highlights them as a safe, robust, and convenient strategy for the dynamic control of therapeutic outputs for future gene- and cell-based precision medicine. Considering that the resveratrol-responsive TtgR, a transcriptional repressor from *P. putida*, might present potential immunogenicity, the potential immunogenicity of RES_{rep}-CAR or RES_{ind}-CAR needs to be further evaluated before clinical trials. In conclusion, our proof of concept and initial in vivo application of two resveratrol-sensitive devices for fine tuning the activity of transgene expression and CAR T cell therapeutic activity illustrates how safe dietary molecules can usher in a new era of precision oncoimmunotherapies.

Materials and Methods

Generation of Stable Cell Lines. The $HEK_{RES\text{-}rep\text{-}SEAP}$ cell line, transgenic for resveratrol-repressed SEAP expression, was constructed by cotransfecting 5×10^4 HEK293 cells with 190 ng of pLF51 (ITR-O_{TRC1}-$P_{hCMVmin}$-SEAP-pA:: P_{hCMV}-TtgR-VPR-P2A-PuroR-pA-ITR) and 10 ng of Sleeping Beauty transposase expression vector pCMV-T7-SB100 (P_{hCMV}-SB100X-pA). The $HEK_{RES\text{-}ind\text{-}SEAP}$ cell line, transgenic for resveratrol-triggered SEAP expression, was constructed by cotransfecting 5×10^4 HEK293 cells with 190 ng of pLF50 (ITR-P_{ResR12}-SEAP-pA::P_{hCMV}-TtgR-KRAB-P2A-PuroR-pA-ITR) and 10 ng of Sleeping Beauty transposase expression vector pCMV-T7-SB100. The $HEK_{RES\text{-}ind\text{-}mut\text{-}SEAP}$ cell line, transgenic for resveratrol-triggered SEAP expression, was constructed by cotransfecting 5×10^4 HEK293 cells with 190 ng of pLF365 (P_{ResR12}-SEAP-pA::P_{hCMV}-TtgR^{H67A}-KRAB-P2A-PuroR-pA-ITR) and 10 ng of Sleeping Beauty transposase expression vector pCMV-T7-SB100. After cultivation with 1 μg/mL puromycin for 2 wk, the monoclonal cell lines were selected and identified.

Lentiviral Transduction and Selection of Stable Cell Lines in Jurkat T and K562 Cells. The $Jurkat_{RES\text{-}ind\text{-}CAR\text{-}EGFP}$ cell line, transgenic for resveratrol-triggered CAR and EGFP expression, was constructed by cotransducing 1×10^5 Jurkat T cells with two lentiviruses: pLF63 (LTR-P_{mPGK}-$ResR_1$-LTR) and pLF64 (LTR-P_{ResR11}-CAR-P2A-EGFP-LTR). Infected Jurkat T cells were cultured for 5 d and then incubated with 10 μM resveratrol for 24 h. EGFP-positive cells were selected based on EGFP fluorescence intensity by FACS-mediated cell sorting using a Becton Dickinson FACSAria Cell Sorter (BD Biosciences). After the EGFP selection, the transduced Jurkat T cells were expanded for further experiments. CD19-negtive K562 target cells, labeled with the EGFP ($CD19^-$ $K562_{EGFP}$) cell line or CD19-positive K562 target cells labeled with the mCherry ($CD19^+$ $K562_{mCherry}$) cell line, were constructed by transducing 1×10^5 K562 cells with lentiviral pLF354 (LTR-$P_{hEF1\alpha}$-EGFP-LTR) or pLF352 (LTR-$P_{hEF1\alpha}$-CD19-mCherry-LTR), respectively. Infected K562 cells were expanded and selected based on EGFP or mCherry fluorescence intensities by FACS-mediated cell sorting using a Becton Dickinson FACSAria Cell Sorter (Becton Dickinson). A Rluc-expressing $CD19^+$ K562 cell line was constructed by transducing $CD19^+$ $K562_{mCherry}$ cells with lentiviral pLF367 (LTR-P_{hEF1a}-Rluc-P2A-PuroR-LTR); the Rluc-expressing cell clones were selected and identified after incubation with 0.5 μg/mL puromycin for 2 wk.

Isolation, Culture, and Transduction of Primary Human $CD4^+$ and $CD8^+$ T Cells. Human peripheral blood mononuclear cells (PBMCs) were isolated from the leukocyte concentrate of the blood from deidentified healthy donors (a byproduct from blood banks in the manufacturing of red blood cell and thrombocyte concentrates from anticoagulated whole blood; Shanghai Blood Center) using Ficoll gradients (Cedarlane Laboratories), as approved by the Medical Ethics Committee of Yangpu Hospital affiliated with Tongji University (approved ID: LL-2018-SCI-003). Primary human $CD4^+$ and $CD8^+$ T cells were then isolated from PBMCs using a $CD4^+$ and $CD8^+$ T cell isolation kit (Miltenyi, 130-045-201 and 130-045-101). T cells were cryopreserved in 90% Roswell Park Memorial Institute (RPMI) 1640 medium and 10% dimethyl sulfoxide (DMSO). Before lentiviral transduction, isolated T cells were thawed, cultured in serum-free hematopoietic cell culture medium X-Vivo 15 (Lonza, 04-418Q), and subsequently activated with anti-CD3/CD28 antibodies (Stem Cell Technologies, 10971) and 50 units/mL recombinant human IL-2 (Peprotech, AF-200-02) for 2 d. Activated primary T cells were resuspended with cell culture medium supplemented with 8 μg/mL polybrene and then transduced with concentrated lentivirus mixture with a multiplicity of infection (MOI) of ~10 for each virus and spun for 90 min at $1,800 \times g$. Infected primary T cells were maintained at a density of $\sim 1 \times 10^6$ cells/mL in X-Vivo 15 medium supplemented with 50 units/mL hIL-2 for 9 d, after which, they were rested and could be used in assays.

Quantification of CAR Expression on T Cells. Jurkat T or primary human T cells were washed, stained with biotin conjugated anti-mouse CD19-specific monoclonal scFv antibodies (FMC63, Bioswan, R19PB-100), followed by streptavidin-phycoerythrin (PE) staining (Bioswan, R19PB-100), and finally stained with a live/dead viability stain. Stained cells were washed three times and then analyzed by flow cytometry. PE fluorescence was quantified by excitation at 561 nm and emission at 586 nm. The percentage of gated cells and their median fluorescence intensity (MFI) were analyzed by the FlowJo software. Weighted CAR expression was evaluated as the percentage of gated cells multiplied by their median fluorescence. Unmodified cells were used as controls.

Quantification of hIL-2 or hIFN-γ Production. Cytokine release assays were performed using hIL-2 or hIFN-γ enzyme-linked immunosorbent assay (ELISA) kits. Engineered Jurkat T cells or human primary T cells were incubated with $CD19^+$-$K562_{mCherry}$ or $CD19^-$-$K562_{EGFP}$ target cells at an effector-to-target (E:T) ratio of 5:1 (5×10^5 cells:1×10^5 cells) in duplicate wells in 96-well flat-bottom plates. After incubation for 18 h, the supernatants were collected and analyzed for human hIL-2 or hIFN-γ by ELISA (BioLegend, 431804 or 430101).

Cytotoxicity Assay of RES_{rep}-CAR or RES_{ind}-CAR Devices in Engineered Primary Human T Cells. $CD19^+$ $K562_{mCherry}$ cells and $CD19^-$ $K562_{EGFP}$ target cells were mixed at a 1:1 ratio and then incubated with primary human T cells expressing RES_{ind}-CAR or RES_{rep}-CAR at an E:T ratio of 10:1 (1×10^6 cells:1×10^5 cells) in 48-well plates. After overnight incubation, cells were washed in cell staining buffer and stained with a Fixable Viability Dye eFluor 660. Stained cells were washed three times and analyzed by BD LSRFortessa flow cytometry. Singlets were gated using forward versus side scatter and followed by gating based on forward scatter area (FSC-H) versus forward scatter height (FSC-A) characteristics. Live cells were gated via the allophycocyanin (APC) channel, and K562 target cells were gated by excluding T cells via the TexasRed channel (mCherry) versus the fluorescein isothiocyanate (FITC) channel (EGFP). Cytotoxicity was calculated by normalization to unmodified T cells (Ctrl). The normalized cytotoxicity was calculated by the following formula:

$$\text{Cytotoxicity}(\%) = \left(1 - \frac{\%CD19^- - K562_{EGFP}\ \text{cells} \,/\, \%CD19^+ - K562_{mCherry}\ \text{cells}}{\%CD19^- - K562_{EGFP}\ \text{cells in control wells} \,/\, \%CD19^+ - K562_{mCherry}\ \text{cells in control wells}}\right) \times 100$$

Animal Experiments.

SEAP production in mice. The $HEK_{RES\text{-}rep\text{-}SEAP}$ and $HEK_{RES\text{-}ind\text{-}SEAP}$ stable cell lines engineered for RES-controlled SEAP repression and expression were

microencapsulated into coherent alginate-poly-(L-lysine)-alginate beads (400 μm diameter; 200 cells/capsule) using a B-395 Pro Encapsulator (BÜCHI Labortechnik AG) according to the manufacturer's instructions. Microcapsules were generated with the following parameters: 0.2-mm nozzle with a vibration frequency of 1,300 Hz, 25-mL syringe at a flow rate of 405 units, and 1.10-kV for bead dispersion. Ten-week-old male wild-type C57BL/6J mice (East China Normal University [ECNU] Laboratory Animal Center) were intraperitoneally implanted with 2×10^6 microencapsulated cells suspended in 800 μL fetal bovine serum (FBS)-free Dulbecco's modified Eagle's medium (DMEM). The mice were then daily intraperitoneally injected with resveratrol at doses ranging from 0 to 500 mg/kg. Blood samples were collected, and SEAP levels were quantified in the serum by using a chemiluminescence-based assay kit (Roche Diagnostics GmbH, 11779842001).

Rapid xenograft tumor model in NCG mice. Female immunodeficient NOD-*Prkdc*^{scid} *Il2rg*^{em26}/NjuCrl (NCG) mice, 6 wk of age, were purchased from Nanjing Biomedical Research Institute of Nanjing University (T001475). NCG mice were initially injected with 3×10^7 target K562 cells (including 1.5×10^7 CD19$^+$ K562$_{mCherry}$ cells and 1.5×10^7 CD19$^-$ K562$_{EGFP}$ cells) intraperitoneally. Ten hours after cell implantation, engineered primary T cells (conventional CAR, RES$_{rep}$-CAR, or RES$_{ind}$-CAR) or unmodified T cells were intraperitoneally injected into mice. The mice were then administrated with resveratrol at doses ranging from 0 to 200 mg/kg/d by intraperitoneal injection, twice each day. Control mice were injected with the vehicle alone. Two days after resveratrol induction, blood samples were collected to determine in vivo cytokine release level using a Cytometric Bead Array (CBA) kit (BD Biosciences 558270 and 560112). Mice were killed by carbon dioxide asphyxiation followed by cervical dislocation. Peritoneal cells were collected based on a procedure described previously (64). Collected cells were centrifuged at $400 \times g$ for 8 min and resuspended in 1 mL of 1× red blood cell lysis solution (Thermo Scientific, 00-4333) for 5 min at room temperature, centrifuged again at $400 \times g$ for 8 min, stained with eFluor 660 conjugated live/dead viability stain, fixed in 4% paraformaldehyde, and finally washed twice and resuspended with cell staining buffer. Samples were analyzed with a BD LSRFortessa cytometer. Data analysis and target cell quantification were performed using FlowJo software (TreeStar), as described for in vitro cell killing experiments. Data plotting and statistical analysis (Student's *t* test) were performed using Prism software (GraphPad).

CD19$^+$ K562 xenograft tumor model in NSG mice. Briefly, female immunodeficient NSG mice (6 wk old) were inoculated with 1×10^6 Rluc-expressing CD19$^+$ K562 cells intravenously. After 5 d, mice were randomly divided into five groups and each mouse was injected with 1×10^7 unmodified T cells (Ctrl), conventional CAR T cells (Conv. CAR), or RES$_{ind}$-CAR T cells, intravenously. Resveratrol was administered intraperitoneally at a dose of 50 mg/kg or by oral administration at a dose of 250 mg/kg. Murine blood was drawn 3 d after T cell infusion, and the secretion of human cytokines in serum was measured using a CBA kit (BD Biosciences, 558270 and 560112). Tumor progression was regularly monitored by bioluminescent imaging (BLI) using an IVIS Lumina imager (PerkinElmer) and quantified as the photon flux over the entire mouse body. For in vivo imaging, each mouse was intraperitoneally injected with 6 mg/kg coelenterazine substrate solution (Yeasen Biotech, Chemical Abstracts Service [CAS] no. 55779-48-1] immediately before imaging.

Ethics. All experiments involving animals were performed in accordance with the protocol approved by the ECNU Animal Care and Use Committee and in direct accord with the Ministry of Science and Technology of the People's Republic of China on Animal Care Guidelines. The protocol used in this study was approved by the ECNU Animal Care and Use Committee (protocol ID: m20160305).

Statistical Analysis. All in vitro data are represented as the mean ± SD of three independent experiments ($n = 3$). For the animal experiments, each treatment group consisted of randomly selected mice ($n = 4$ to 6). Blood sample analysis was blinded. Comparisons between groups were performed using Student's *t* test, and the results are expressed as means ± SEM. Differences were considered statistically significant at $P < 0.05$. Prism 6 software (GraphPad Software, Inc.) was used for statistical analysis. *n* and *P* values are indicated in the figure legends.

Data Availability. All data needed to evaluate the conclusions in the paper are present in the paper and/or *SI Appendix, Supplementary Methods*. All genetic components related to this paper are available with a material transfer agreement and can be requested from H.Y. (hfye@bio.ecnu.edu.cn).

ACKNOWLEDGMENTS. We thank the excellent scientific and technical assistance of the Flow Cytometry Core Facility staff of ECNU for their help with flow cytometry. This work was financially supported by grants from the National Key R&D Program of China, Synthetic Biology Research (no. 2019YFA0904500), the National Natural Science Foundation of China (nos. 31971346 and 31861143016), the Science and Technology Commission of Shanghai Municipality (no. 18JC1411000), and the Fundamental Research Funds for the Central Universities to H.Y. This work was also partially supported by the Natural Science Foundation of Shanghai (grant no. 18ZR1436000) to F.C. We also thank the ECNU Multifunctional Platform for Innovation (011) for supporting the mice experiments and the Instruments Sharing Platform of the School of Life Sciences, ECNU.

1. C. H. June, R. S. O'Connor, O. U. Kawalekar, S. Ghassemi, M. C. Milone, CAR T cell immunotherapy for human cancer. *Science* **359**, 1361–1365 (2018).
2. N. N. Shah, T. J. Fry, Mechanisms of resistance to CAR T cell therapy. *Nat. Rev. Clin. Oncol.* **16**, 372–385 (2019).
3. M. Sadelain, R. Brentjens, I. Rivière, The basic principles of chimeric antigen receptor design. *Cancer Discov.* **3**, 388–398 (2013).
4. S. S. Neelapu *et al.*, Axicabtagene ciloleucel CAR T-cell therapy in refractory large B-cell lymphoma. *N. Engl. J. Med.* **377**, 2531–2544 (2017).
5. S. L. Maude *et al.*, Tisagenlecleucel in children and young adults with B-cell lymphoblastic leukemia. *N. Engl. J. Med.* **378**, 439–448 (2018).
6. C. J. Turtle *et al.*, Durable molecular remissions in chronic lymphocytic leukemia treated with CD19-specific chimeric antigen receptor-modified T cells after failure of ibrutinib. *J. Clin. Oncol.* **35**, 3010–3020 (2017).
7. J. A. Fraietta *et al.*, Determinants of response and resistance to CD19 chimeric antigen receptor (CAR) T cell therapy of chronic lymphocytic leukemia. *Nat. Med.* **24**, 563–571 (2018).
8. K. T. Roybal, W. A. Lim, Synthetic immunology: Hacking immune cells to expand their therapeutic capabilities. *Annu. Rev. Immunol.* **35**, 229–253 (2017).
9. S. Rafiq, C. S. Hackett, R. J. Brentjens, Engineering strategies to overcome the current roadblocks in CAR T cell therapy. *Nat. Rev. Clin. Oncol.* **17**, 147–167 (2020).
10. M. L. Davila *et al.*, Efficacy and toxicity management of 19-28z CAR T cell therapy in B cell acute lymphoblastic leukemia. *Sci. Transl. Med.* **6**, 224ra25 (2014).
11. J. Gust *et al.*, Endothelial activation and blood–brain barrier disruption in neurotoxicity after adoptive immunotherapy with CD19 CAR-T cells. *Cancer Discov.* **7**, 1404–1419 (2017).
12. C. J. Turtle *et al.*, Immunotherapy of non-Hodgkin's lymphoma with a defined ratio of CD8$^+$ and CD4$^+$ CD19-specific chimeric antigen receptor–modified T cells. *Sci. Transl. Med.* **8**, 355ra116 (2016).
13. J. H. Park *et al.*, Long-term follow-up of CD19 CAR therapy in acute lymphoblastic leukemia. *N. Engl. J. Med.* **378**, 449–459 (2018).
14. K. Mestermann *et al.*, The tyrosine kinase inhibitor dasatinib acts as a pharmacologic on/off switch for CAR T cells. *Sci. Transl. Med.* **11**, eaau5907 (2019).
15. M.-R. Wu, B. Jusiak, T. K. Lu, Engineering advanced cancer therapies with synthetic biology. *Nat. Rev. Cancer* **19**, 187–195 (2019).
16. M. J. Brenner, J. H. Cho, N. M. L. Wong, W. W. Wong, Synthetic biology: Immunotherapy by design. *Annu. Rev. Biomed. Eng.* **20**, 95–118 (2018).
17. A. Di Stasi *et al.*, Inducible apoptosis as a safety switch for adoptive cell therapy. *N. Engl. J. Med.* **365**, 1673–1683 (2011).
18. T. Sato *et al.*, Engineered human tmpk/AZT as a novel enzyme/prodrug axis for suicide gene therapy. *Mol. Ther.* **15**, 962–970 (2007).
19. X. Wang *et al.*, A transgene-encoded cell surface polypeptide for selection, in vivo tracking, and ablation of engineered cells. *Blood* **118**, 1255–1263 (2011).
20. B. Philip *et al.*, A highly compact epitope-based marker/suicide gene for easier and safer T-cell therapy. *Blood* **124**, 1277–1287 (2014).
21. G. Giordano-Attianese *et al.*, A computationally designed chimeric antigen receptor provides a small-molecule safety switch for T-cell therapy. *Nat. Biotechnol.* **38**, 426–432 (2020).
22. B. Zhang *et al.*, Photoswitchable CAR-T cell function in vitro and in vivo via a cleavable mediator. *Cell Chem. Biol.* **28**, 60–69.e7 (2021).
23. C.-Y. Wu, K. T. Roybal, E. M. Puchner, J. Onuffer, W. A. Lim, Remote control of therapeutic T cells through a small molecule-gated chimeric receptor. *Science* **350**, aab4077 (2015).
24. R. Sakemura *et al.*, A Ttet-Oon inducible system for controlling CD19-chimeric antigen receptor expression upon drug administration. *Cancer Immunol. Res.* **4**, 658–668 (2016).
25. H. Li *et al.*, Engineering clinically-approved drug gated CAR circuits. *bioRxiv* [Preprint] (2020). https://doi.org/10.1101/2020.12.14.419812 (Accessed 14 December 2020).
26. M. Jan *et al.*, Reversible ON- and OFF-switch chimeric antigen receptors controlled by lenalidomide. *Sci. Transl. Med.* **13**, eabb6295 (2021).
27. E. W. Weber *et al.*, Transient rest restores functionality in exhausted CAR-T cells through epigenetic remodeling. *Science* **372**, eaba1786 (2021).
28. D. T. Rodgers *et al.*, Switch-mediated activation and retargeting of CAR-T cells for B-cell malignancies. *Proc. Natl. Acad. Sci. U.S.A.* **113**, E459–E468 (2016).
29. S. Viaud *et al.*, Switchable control over in vivo CAR T expansion, B cell depletion, and induction of memory. *Proc. Natl. Acad. Sci. U.S.A.* **115**, E10898–E10906 (2018).
30. J. H. Cho, J. J. Collins, W. W. Wong, Universal chimeric antigen receptors for multiplexed and logical control of T cell responses. *Cell* **173**, 1426–1438.e11 (2018).

31. Y. Pan *et al*., Mechanogenetics for the remote and noninvasive control of cancer immunotherapy. *Proc. Natl. Acad. Sci. U.S.A.* **115**, 992–997 (2018).
32. Z. Huang *et al*., Engineering light-controllable CAR T cells for cancer immunotherapy. *Sci. Adv.* **6**, eaay9209 (2020).
33. L. He *et al*., Circularly permuted LOV_2 as a modular photoswitch for optogenetic engineering. *Nat. Chem. Biol.* **17**, 915–923 (2021).
34. K. T. Roybal *et al*., Precision tumor recognition by T cells with combinatorial antigen-sensing circuits. *Cell* **164**, 770–779 (2016).
35. J. Z. Williams *et al*., Precise T cell recognition programs designed by transcriptionally linking multiple receptors. *Science* **370**, 1099–1104 (2020).
36. R. A. Hernandez-Lopez *et al*., T cell circuits that sense antigen density with an ultrasensitive threshold. *Science* **371**, 1166–1171 (2021).
37. A. Hyrenius-Wittsten *et al*., SynNotch CAR circuits enhance solid tumor recognition and promote persistent antitumor activity in mouse models. *Sci. Transl. Med.* **13**, eabd8836 (2021).
38. J. H. Choe *et al*., SynNotch-CAR T cells overcome challenges of specificity, heterogeneity, and persistence in treating glioblastoma. *Sci. Transl. Med.* **13**, eabe7378 (2021).
39. J. A. Baur *et al*., Resveratrol improves health and survival of mice on a high-calorie diet. *Nature* **444**, 337–342 (2006).
40. D. Sinha, N. Sarkar, J. Biswas, A. Bishayee, Resveratrol for breast cancer prevention and therapy: Preclinical evidence and molecular mechanisms. *Semin. Cancer Biol.* **40–41**, 209–232 (2016).
41. L. Huminiecki, J. Horbańczuk, The functional genomic studies of resveratrol in respect to its anti-cancer effects. *Biotechnol. Adv.* **36**, 1699–1708 (2018).
42. M. G. Novelle, D. Wahl, C. Diéguez, M. Bernier, R. de Cabo, Resveratrol supplementation: Where are we now and where should we go? *Ageing Res. Rev.* **21**, 1–15 (2015).
43. S. L. Ramírez-Garza *et al*., Health effects of resveratrol: Results from human intervention trials. *Nutrients* **10**, 1892 (2018).
44. D. Xiong *et al*., Improving key enzyme activity in phenylpropanoid pathway with a designed biosensor. *Metab. Eng.* **40**, 115–123 (2017).
45. A. Chavez *et al*., Highly efficient Cas9-mediated transcriptional programming. *Nat. Methods* **12**, 326–328 (2015).
46. J. H. Ko *et al*., The role of resveratrol in cancer therapy. *Int. J. Mol. Sci.* **18**, 1–36 (2017).
47. L. G. Carter, J. A. D'Orazio, K. J. Pearson, Resveratrol and cancer: Focus on in vivo evidence. *Endocr. Relat. Cancer* **21**, R209–R225 (2014).
48. M. Craveiro *et al*., Resveratrol stimulates the metabolic reprogramming of human $CD4^+$ T cells to enhance effector function. *Sci. Signal.* **10**, 1–15 (2017).
49. K. T. Noh *et al*., Resveratrol regulates naïve $CD8^+$ T-cell proliferation by upregulating IFN-γ-induced tryptophanyl-tRNA synthetase expression. *BMB Rep.* **48**, 283–288 (2015).
50. C. Daniels, A. Daddaoua, D. Lu, X. Zhang, J. L. Ramos, Domain cross-talk during effector binding to the multidrug binding TTGR regulator. *J. Biol. Chem.* **285**, 21372–21381 (2010).
51. S. Jones *et al*., Lentiviral vector design for optimal T cell receptor gene expression in the transduction of peripheral blood lymphocytes and tumor-infiltrating lymphocytes. *Hum. Gene Ther.* **20**, 630–640 (2009).
52. A. M. Fernandez-Escamilla, G. Fernandez-Ballester, B. Morel, S. Casares-Atienza, J. L. Ramos, Molecular binding mechanism of TtgR repressor to antibiotics and antimicrobials. *PLoS One* **10**, e0138469 (2015).
53. J. Yin *et al*., A green tea-triggered genetic control system for treating diabetes in mice and monkeys. *Sci. Transl. Med.* **11**, 1–15 (2019).
54. J. Shao *et al*., Smartphone-controlled optogenetically engineered cells enable semiautomatic glucose homeostasis in diabetic mice. *Sci. Transl. Med.* **9**, 1–14 (2017).
55. M. Xie *et al*., β-cell-mimetic designer cells provide closed-loop glycemic control. *Science* **354**, 1296–1301 (2016).
56. H. Ye *et al*., Self-adjusting synthetic gene circuit for correcting insulin resistance. *Nat. Biomed. Eng.* **1**, 0005 (2017).
57. S. Xue *et al*., A synthetic-biology-inspired therapeutic strategy for targeting and treating hepatogenous diabetes. *Mol. Ther.* **25**, 443–455 (2017).
58. Y. Liu *et al*., Immunomimetic designer cells protect mice from MRSA infection. *Cell* **174**, 259–270.e11 (2018).
59. L. Nissim *et al*., Synthetic RNA-based immunomodulatory gene circuits for cancer immunotherapy. *Cell* **171**, 1138–1150.e15 (2017).
60. W. C. Ruder, T. Lu, J. J. Collins, Synthetic biology moving into the clinic. *Science* **333**, 1248–1252 (2011).
61. M. Xie, M. Fussenegger, Designing cell function: Assembly of synthetic gene circuits for cell biology applications. *Nat. Rev. Mol. Cell Biol.* **19**, 507–525 (2018).
62. X. Xiong, M. Chen, W. A. Lim, D. Zhao, L. S. Qi, CRISPR/Cas9 for human genome engineering and disease research. *Annu. Rev. Genomics Hum. Genet.* **17**, 131–154 (2016).
63. J. N. Kochenderfer *et al*., Eradication of B-lineage cells and regression of lymphoma in a patient treated with autologous T cells genetically engineered to recognize CD19. *Blood* **116**, 4099–4102 (2010).
64. A. Ray, B. N. Dittel, Isolation of mouse peritoneal cavity cells. *J. Vis. Exp.* **35**, 1488 (2010).